Available online at www.sciencedirect.com

ScienceDirect

Procedia Engineering 114 (2015) 232 – 239

Procedia Engineering

www.elsevier.com/locate/procedia

1st International Conference on Structural Integrity

Comparison between Finite Element Method Simulation, Digital Image Correlation and Strain Gauges measurements in a 3-Point Bending Flexural Test

Tiago Ramos[a]*, Daniel F. O. Braga[a], Shayan Eslami[a], Paulo J. Tavares[a], P. M. G. P. Moreira[a]

[a]*INEGI – Institute of Science and Innovation in Mechanical and Industrial Engineering, 4200-465 Porto, Portugal*

Abstract

Mechanical testing holds a decisive role in structural components design. It supports and validates computer simulation models, spots design failures or critical sections and reveals the structure real behavior under static or dynamic loads. In order to reduce weight and/or improve durability of a train passenger car underframe, an alternative design was proposed based on an aluminium alloy modular components joined by laser beam welding. A section of this prototype was tested, according to a three-point bending flexural test configuration, and monitored with both optic techniques, such as digital image correlation and electric strain gauges. After processing, the resultant data was compared with the finite element method analysis for simulation model validation and structure inspection.

Peer-review under responsibility of INEGI - Institute of Science and Innovation in Mechanical and Industrial Engineering

Keywords: LighTRAIN, Digital Image Correlation, DIC, Finite Element Method Simulation, FEM, Platform, Train, Bending, Flex, Test, Laser Beam Welding, LBW, Aluminium

* Corresponding author. Tel.: +351–22–9578710; fax: +351–22–9537352.
E-mail address: tramos@inegi.up.pt

Peer-review under responsibility of INEGI - Institute of Science and Innovation in Mechanical and Industrial Engineering
doi:10.1016/j.proeng.2015.08.063

1. Introduction

In order to reduce weight and/or improve durability of a train passenger car underframe, an alternative design was proposed based on an aluminium alloy modular components joined by laser beam welding (LBW).

After construction, the underframe was tested according to a three-point flexural test, in a modular servo-hydraulic INSTRON® machine.

Nomenclature

ε_{xx}	Strain in the x direction
ε_{yy}	Strain in the y direction
Ø	Diameter
ν	Poisson's ratio
E	Young Modulus

2. Test Description and Equipment Setup

A three-point bending flexural test is characterized by the application of a load, in a test specimen supported by two different points, symmetrical to the load application section. For this case, the prototype was disposed over two steel rails and compressed in its center by a steel cylinder attached to the hydraulic actuator as seen in Fig. 1, in order to guarantee a uniform load distribution along the underframe, as required by the test design. Although the INSTRON® machine is equipped with a load cell and a linear variable differential transformer (LVDT) sensor capable of providing a force-displacement curve, representative of the underframe stiffness, it was found relevant to monitor specific sections of the prototype external surfaces. In order to do this, two different techniques were chosen: While digital image correlation (DIC) is capable of providing (almost) continuous displacement and strain fields of deformed surfaces it is more susceptible to noise when regarding strain estimation. This is mainly due to the fact that, in this technique, strains are determined indirectly through differentiation of the measured displacement data. On the other hand, discrete sensors, such as strain gauges have proven to be a mature technique for structural health monitoring (SHM), with low relative errors. The cylinder, rails supports and monitored areas, by the different techniques, can be found in Fig. 1. All the dimensions in it indicated are expressed in millimeters.

The rails relative distance was defined in order to assure a large tested area, representative of the whole prototype behaviour, and still guarantee a good sensitivity in the available 250kN INSTRON® load cell. Since this sensor output bandwidth was -10V/10V for a 0kN to 250kN applied load, in order to guarantee at least a ~0.5V signal variation for a maximum expected measured load of 6.5kN, the rails were positioned at 1480mm apart, as it was predicted by the numerical model.

The test was performed with a vertical displacement control, at 0.1mm/s, with 0.5mm steps from 0mm to 3.5mm displacement and after, with 1mm steps until a maximum of 6.5mm displacement was achieved.

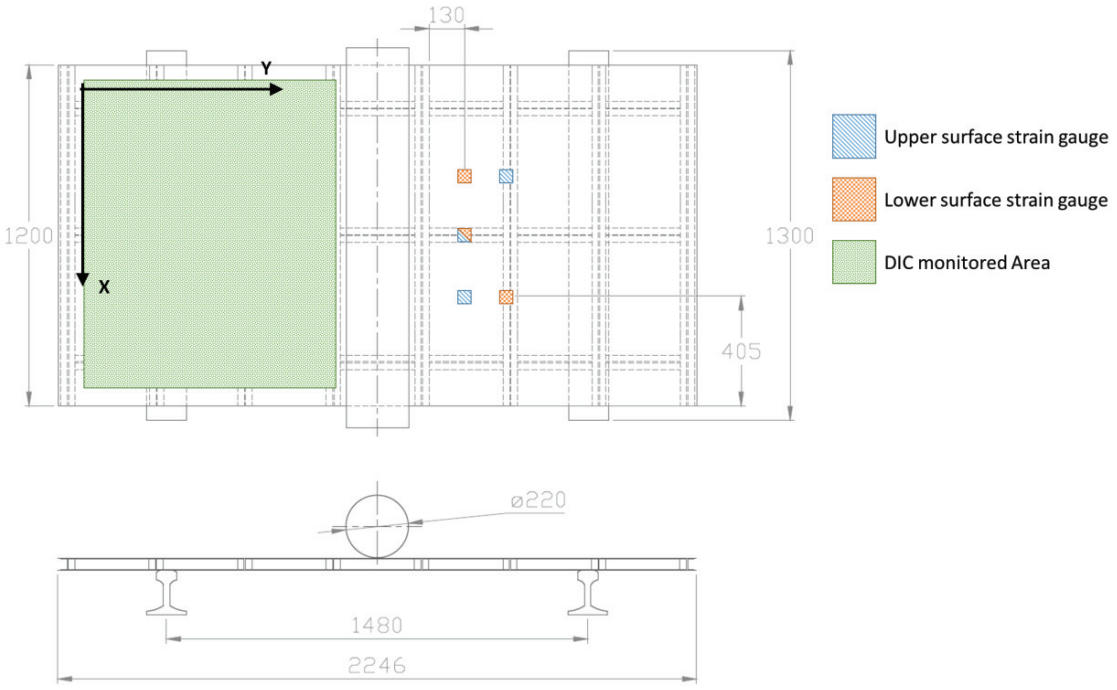

Fig. 1: Cylinder, rail supports position and monitored areas.

2.1. Strain gauges Setup

Each electrical strain gauge used was composed by a Tee Rosette that measures strain in two perpendicular directions. The 6 different strain gauges pairs recorded the strain in the x and y direction (ε_{xx} and ε_{yy}) in real time, synchronized with the analogic signals (load and displacement) from the INSTRON® load cell and LVDT, while the DIC images were captured after stopping the hydraulic machine in every test step. The signals from the strain gauges and the INSTRON® sensors were connected to a National Instruments™ acquisition system, which in turn was connected to a laptop computer.

The strain gauges used were a 120Ω±0.4% Tee Rosette for general purposes with the reference code: CEA-13-125UT-120 from Vishay™ - Micro Measurements. The strain gauges errors returned by a strain gauge tester were found to be between 0.5% and 2%, when compared with a nominal resistance of 120Ω. The sensors were assembled using a quarter-bridge configuration for wire resistance compensation.

As it was previously mentioned and shown in Fig. 1 three of the strain gauges were positioned in the upper surface of the prototype while the remaining ones in the lower surface.

It is important to mention that the strain gauges *e4* and *e5* presented a technical problem, while positioning the underframe in the rails support, which caused them to be ripped off. After being repaired, they were tested and showed to behave in a similar way to the remaining ones. This was still taken in consideration when analysing the strain data as a possible reason for unsatisfactory results.

2.2. DIC Setup

The equipment used to capture and process the images for DIC analysis was the Vic-3D™ system from Correlated Solutions equipped with two Schneider-Kreuznach 16mm focal distance lenses. The two 4.1MPixel CMOSIS cameras were positioned at 1800mm from the underframe surface at 870mm distance, performing an aperture angle of approximately 27° as it shown in Fig. 2.

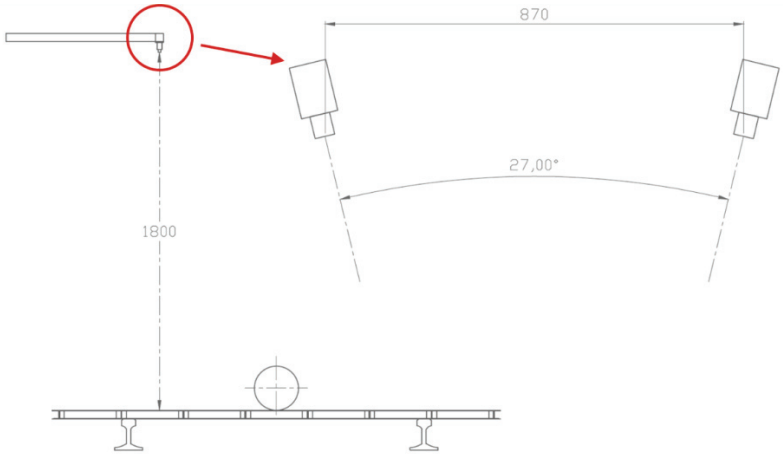

Fig. 2: DIC cameras position and orientation.

In order to properly acquire and process images for DIC applications a random speckle pattern has to be firstly applied in the test specimen. This is commonly done by applying a sprayed black ink over a smooth white layer. Due to the large dimensions of the object, and in order to assure a 3 to 8 image pixels per dot ratio an alternative technique is commonly used by the present research group: After applying a white layer of ink over half the specimen, a vinyl (polyvinyl chloride) stencil made of 4mm diameter independent dots was transferred to the prototype surface. Blank areas due to imperfections in the transferred process were filled with a black marker with the same diameter. The final result of this application is presented in Fig. 3 (a). After selecting the region of interest (ROI) presented in Fig. 3 (b) the images were processed using the Vic-3D™ software from Correlated Solution. The chosen processing parameters are presented in Table 1.

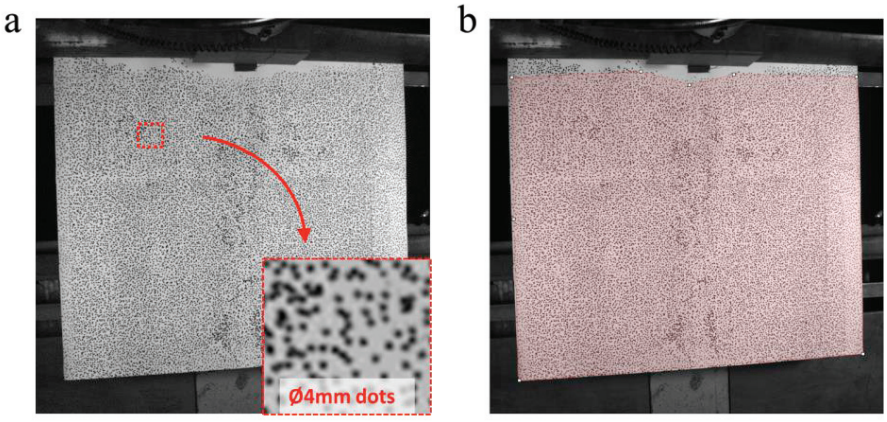

Fig. 3: (a) vinyl random speckle pattern in the prototype for DIC application; (b) selected ROI.

Table 1: Displacement and strain processing parameters in Vic-3D ™software

Vic - 3D Analysis Option	
Correlation criterion	Normalized Squared Differences
Interpolation method	Optimized 8-tap
Subset weights	Gaussian
Subset size	29 Pixel
Step size	3 Pixel
Low-pass filter images	Yes
Strain tensor type	Lagrangian
Strain computation filter size	95

3. Test Results

After image processing, it is possible to infer about the underframe geometrical condition before, during and after the test. Fig. 4 displays a tridimensional representation and its vertical projection of the prototype monitored area. The digital surface reconstruction was made by the DIC software based on stereography principles. As it can be seen, the upper surface of the underframe already presented some spatial distortions, explained for instance by the complex welding procedure. Some of the areas still inside the ROI, marked with a dashed line in Fig. 4, could not be processed by the DIC algorithm. This may be explained by low speckle density, the possibility of those areas being out of the camera depth of view, or insufficient data during the bundle calibration that precludes a solid epipolar constrain in those sections. Please note that the 3D representation in Fig. 4 is not in the scale (in the Z/vertical direction), in order to easily distinguish out-of-plane distortions.

The remaining deformed images can be used to make a computer reconstruction of the model behaviour during the test, to evaluate spatial displacement and strain fields and principal strain directions. In Fig. 5 a 3D reconstruction of three moments of the test is presented. In this image the steel cylinder position is aligned, parallel and closer to the lower section in the right image. The three moments concern the reference state (absence of axial load), a 3mm and 6.5mm actuator displacement respectively.

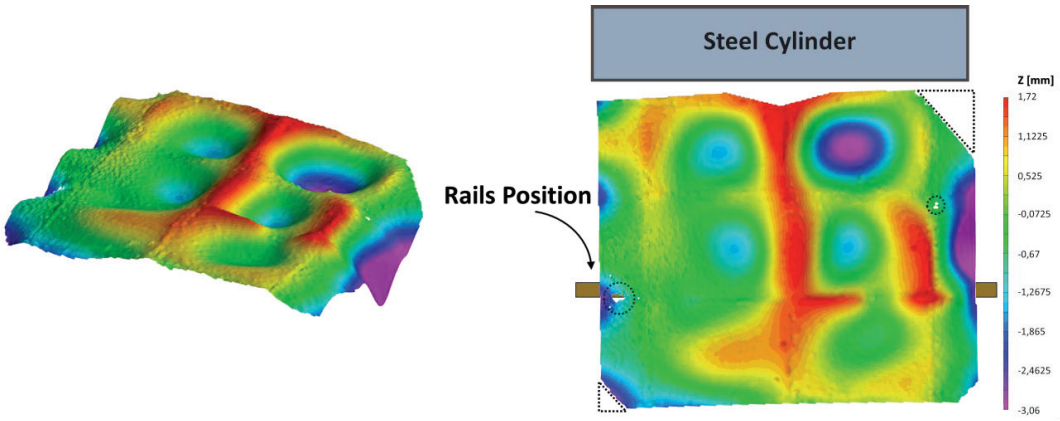

Fig. 4: Surface distortion before the test. Measurements made in the reference image. Dashed lines mark blank spots, common for all the measurements with lack of information.

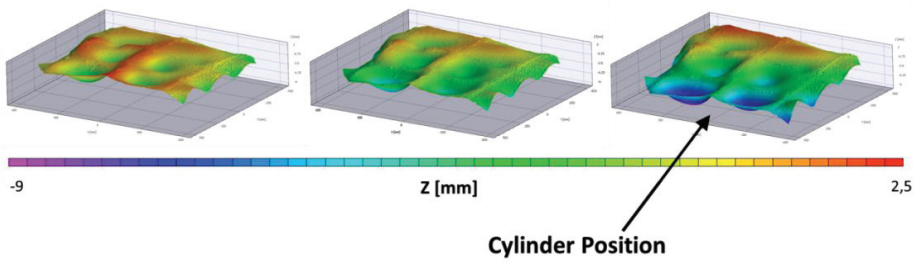

Fig. 5: Prototype surface displacement evolution over the test. Undeformed image (Left), 3mm cylinder displacement (Centre) and 6.5mm cylinder displacement (Right).

Since the strain gauges data was captured in real time, the different test phases were identified and averaged during the prototype "resting time". The strain measurements can be seen in Fig. 6, where the legend refers the strain gauges position marked with the prefix "e" in **Error! Reference source not found.**. The suffix "x" and "y" concern the measured direction according to the referential in Fig. 1.

As it was expected, the strains in the y direction were higher than the ones in the x, and all the strain measurements returned to its initial value (zero) after unloading the specimen.

4. Numerical modeling

A numerical model of the prototype was developed through *Abaqus*® finite element method (FEM) software, in order to define testing conditions, as well as for comparison purposes. The model was composed of 4 different geometric parts (transversal profile, longitudinal profile, plate and actuator), as it may be observed in Fig. 7 (a). The actuator was modelled as an analytic rigid shell, while the rest of the components were modelled as elastic homogeneous. The material properties used were the ones available in the AA6082-T6 datasheets (E=69GPa and ν=0.33). A FEM mesh was applied using both linear and quadratic 3D stress elements with reduced integration. In total the mesh is composed of 99730 linear hexahedral elements (C3D8R) and 84851 quadratic hexahedral elements (C3D20R), adding up to 674369 nodes in total. The welded connections were modelled using tie constrains along the profiles with a widths of 3 mm (from visual inspection of the prototype), in similar positions regarding the prototype tested as in Fig. 7 (b).

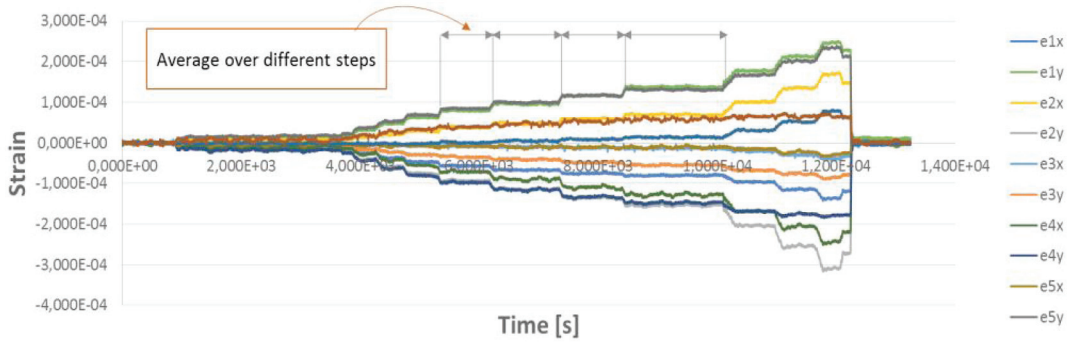

Fig. 6: Strain gauges results over time during the 3-point flexural test.

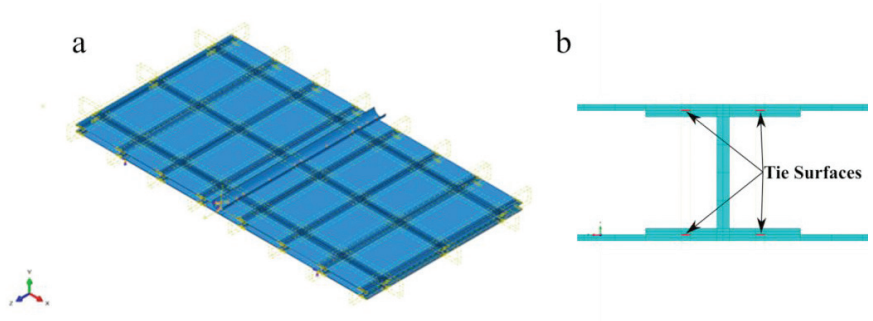

Fig. 7: FEM model geometry, restraining conditions and loading.

Strain data was extracted using element sets positioned similarly to the strain gauges positions and *History Output*, in order to have this data throughout the loading stage.

5. Results comparison and analysis

After the test, the numerical modelling results for the prototype surface displacement and strains were compared with both DIC and strain gauges measurements. An example of this comparison is shown below in Fig. 8.

The main differences between DIC and strain gauges measurements may be explained by the following factors:

- Lack of symmetry in the prototype.
- Strain calculation limitation in digital image correlation algorithms.
- Inconsistence in the weld beads.
- Distortions, clearances and gaps in the prototype surfaces, due to low initial construction tolerance requirements.
- Noise in the strain gauges signal that could affect averaging operations.
- Noise propagation in averaging operations.
- Technical problems as the ones mentioned for the *e4* and *e5* strain gauges.

The measured load evolution with the actuator cylinder vertical displacement can be found in Table 2 for both the experimental (from the INSTRON® load cell) and the FEM simulation results.

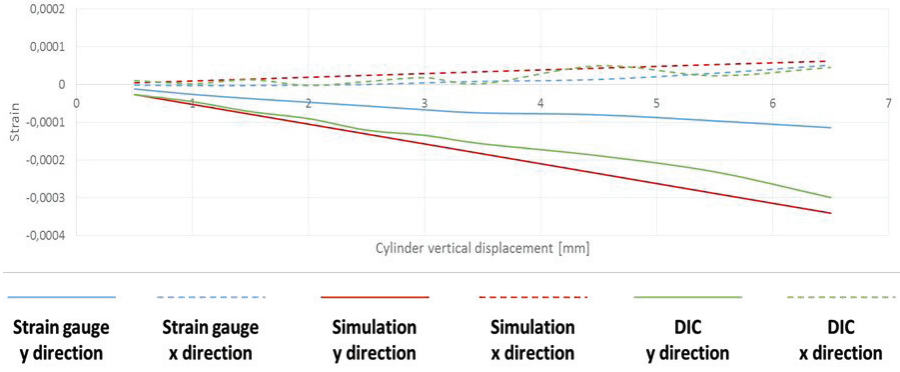

Fig. 8: Strain gauge, DIC and numerical model results for the strain gauge *e1*.

Table 2: Experimental Load and FEM Simulation Load evolution with the actuator vertical displacement along the different test steps

Cylinder Vertical Displacement [mm]	Experimental Load [kN]	FEM Load [kN]
0	0	0,0
0,5	1	1,0
1	1,5	2,0
1,5	1,9	3,0
2	2,4	4,0
2,5	2,5	5,1
3	3,4	6,1
3,5	3,9	7,1
4,5	5	9,1
5,5	6,3	11,1
6,5	7,5	13,1

On the other hand, the differences between the measurements (by both DIC and strain gauges techniques) and the Abaqus® simulation may be explained by:

- Distortions, clearances and gaps in the prototype surfaces, due to low initial construction tolerance requirements.
- Inexistence of a perfect weld seam connection. The model included a perfect solidarity between the degrees of freedom in the welded surfaces.
- Mechanical properties transformations, due to the welding process, were not taken in consideration in the model.

Fig. 9 illustrates the differences between the *Abaqus*® simulation and the measured results for the last monitored step of the test. As it can be seen the main differences are concentrated in the transverse aluminium profiles closer to the steel cylinder position.

6. Conclusions

The good correlation between DIC and strain gauges, verifies that DIC is a practicable and reliable method for structural heath monitoring, being its main advantage related with its capability for full-field assessments.

The initial DIC measured distortions and the overall lower performance of the prototype, when compared with the FEM simulation, suggested that CO_2 laser beam welding is not the most viable manufacture process for lightweight aluminum structures.

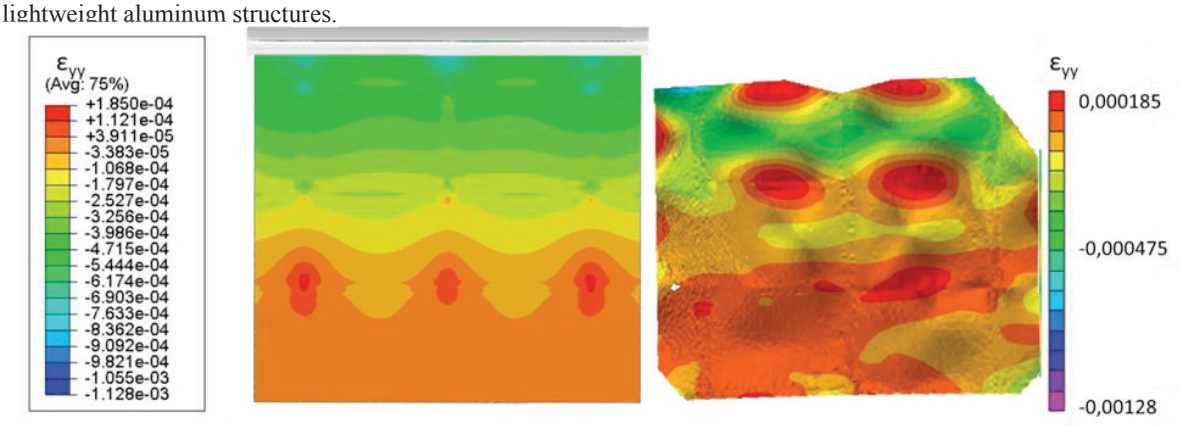

Fig. 9: Strain in *y* direction (ε_{yy}) comparison between simulation and DIC measurements for the last monitored step.